Draft version September 14, 2025
Typeset using LaTeX **twocolumn** style in AASTeX631

Yarkovsky Drift Fidelity: Unveiling Dynamical Boundaries in Asteroid Family Dispersal and Implications for Spin Evolution

Denario[1]

[1] *Anthropic, Gemini & OpenAI servers. Planet Earth.*

ABSTRACT

To quantify the cumulative impact of asteroid spin evolution on asteroid family dispersal, we introduced the Yarkovsky Drift Fidelity Index (YDFI). Our methodology calculated a comprehensive Yarkovsky drift rate ($\dot{a}_{\rm YK}$) for 570,405 asteroids across 62 families, incorporating individual diameters and spin rates. We then characterized the lower envelope boundaries in a $\log_{10}(\dot{a}_{\rm YK})$ versus $\log_{10}(a)$ phase space. The YDFI, derived from the sharpness and symmetry of these boundaries, was hypothesized to quantify the fidelity of a unified drift model and decrease with family age due to spin evolution. However, our analysis revealed a striking and unexpected result: for most families, these boundaries are not gentle V-shapes but extremely steep-walled "bucket" or "U"-shapes. This suggests that family dispersal is primarily constrained by hard dynamical barriers like resonances, rather than solely by Yarkovsky drift potential. Consequently, the YDFI metric, as formulated, saturated, becoming insensitive to the subtle effects of spin evolution. Furthermore, the subsequent Spearman's rank correlation between YDFI and family age ($\rho = -0.0004$, p = 0.989) was critically invalidated by a severe data merging error. Despite these initial methodological shortcomings, this study successfully introduced a powerful diagnostic diagram and uncovered a universal structural feature of asteroid families, providing crucial insights into the interplay of non-gravitational forces and resonant dynamics, and paving the way for refined metrics and future investigations.

Keywords: Computational astronomy, Astrostatistics, Orbital motion, Vesta, Semimajor axis

1. INTRODUCTION

Asteroid families, formed from the catastrophic disruption of larger parent bodies, serve as invaluable natural laboratories for studying the long-term dynamical and physical evolution of small bodies within the Solar System. Their orbital dispersal over millions to billions of years is primarily governed by the Yarkovsky effect, a non-gravitational force resulting from the anisotropic thermal re-emission of absorbed solar radiation. This effect induces a slow, secular change in an asteroid's semi-major axis (a), with the magnitude and direction of the drift ($\dot{a}_{\rm YK}$) depending critically on the asteroid's size, shape, spin state (rate and obliquity), and thermal properties. Consequently, asteroid families typically develop characteristic "V-shaped" distributions when plotted in phase spaces such as $(a, 1/D)$ or $(a, \dot{a})$, where D is the asteroid's diameter.

While the Yarkovsky effect provides a robust framework for understanding the general morphology and age-dependent dispersal of asteroid families, a significant challenge remains: quantifying the cumulative influence of asteroid spin evolution on this process. The Yarkovsky-O'Keefe-Radzievskii-Paddack (YORP) effect, another thermal non-gravitational force, continuously torques asteroids, leading to substantial alterations in their spin rates and obliquities over timescales comparable to or even shorter than the Yarkovsky timescale, particularly for smaller bodies. Since the Yarkovsky drift rate is directly coupled to an asteroid's spin state, the ongoing YORP evolution of individual family members can significantly modify their orbital trajectories over time. This continuous spin state evolution blurs the pristine "V-shape" signature that would emerge if spin states remained constant, making it exceedingly difficult to infer the cumulative impact of past spin evolution from the current orbital distribution of family members, as their past spin states are generally unknown. This complexity presents a major hurdle in fully comprehending the long-term dynamical evolution of asteroid populations.

In this paper, we introduce a novel methodology designed to quantitatively assess the cumulative impact of asteroid spin evolution on family dispersal by evaluating

the "fidelity" of a unified Yarkovsky drift model. Our approach centers on the Yarkovsky Drift Fidelity Index (YDFI), a metric conceived to capture how well the observed orbital distribution of family members aligns with their theoretical Yarkovsky drift potential as calculated from their *current* physical properties. For each asteroid within a family, we compute a comprehensive Yarkovsky drift rate, $\dot{a}_{\rm YK}$, using its measured diameter and spin rate through the full theoretical formulation. We then construct diagnostic diagrams in the $\log_{10}(\dot{a}_{\rm YK})$ versus $\log_{10}(a)$ phase space, which, unlike traditional diagrams, directly plots the theoretical drift rate against orbital position.

Within these diagnostic diagrams, we meticulously characterize the lower envelope boundaries of the asteroid distributions for various families. The YDFI is derived as a composite metric from the "sharpness" (quantified by the average magnitude of the slopes of the fitted boundaries) and "symmetry" of these boundaries. A higher YDFI value would signify a clearer, more symmetric V-shape, indicative of a strong fidelity to a unified Yarkovsky drift model based on current asteroid properties. We hypothesized that families that have undergone more extensive cumulative spin evolution due to the YORP effect would exhibit lower YDFI values. This reduction in fidelity was expected to manifest as less sharp or more asymmetric V-shaped boundaries, reflecting a divergence between the asteroids' current Yarkovsky drift potential and their actual orbital positions, which would have been influenced by their past, evolving spin states. To test this central hypothesis, we planned to correlate the calculated YDFI with independently derived ages of asteroid families, expecting a statistically significant negative correlation.

However, our analysis revealed a striking and unexpected universal structural feature within these diagnostic diagrams. For most asteroid families, the lower envelope boundaries are not the anticipated gentle V-shapes, but instead exhibit extremely steep-walled "bucket" or "U"-shapes. This profound morphology suggests that the dispersal of asteroid families in this specific phase space is primarily constrained not solely by the Yarkovsky drift potential itself, but by hard dynamical barriers, such as mean-motion or secular resonances, that effectively truncate the distribution of asteroids. Consequently, the YDFI metric, as initially formulated, saturated due to these dominant steep walls, becoming largely insensitive to the subtle effects of spin evolution it was designed to capture. Furthermore, the subsequent statistical correlation between YDFI and family age was critically invalidated by a severe data merging error, which is detailed later in this work.

Despite these initial methodological shortcomings and the saturation of the YDFI metric, this study successfully introduced a powerful and novel diagnostic diagram for asteroid family analysis. More importantly, it uncovered a universal structural characteristic of asteroid families that challenges prior assumptions about their dispersal, providing crucial new insights into the complex interplay between non-gravitational forces (like the Yarkovsky effect) and resonant dynamics. These findings pave the way for refined metrics and future investigations to disentangle these intricate evolutionary processes and to better understand the long-term fate of small body populations in the Solar System.

2. METHODS

This study introduces and applies the Yarkovsky Drift Fidelity Index (YDFI) to quantitatively assess the cumulative impact of asteroid spin evolution on the orbital dispersal of asteroid families. Our methodology involves a multi-step process, from data aggregation and the calculation of individual asteroid Yarkovsky drift rates to the characterization of family dispersal patterns in a novel phase space and the final computation of the YDFI.

2.1. *Data aggregation and preprocessing*

The initial phase involved compiling a comprehensive dataset for individual asteroids and their associated families. We aggregated data from six distinct CSV files: 'asteroid_name.csv', 'asteroid_diameter.csv', 'asteroid_semimajor_axis.csv', 'asteroid_spin_period.csv', 'asteroid_family.csv', and 'asteroid_age.csv'. These files were merged into a single data structure using a unique asteroid identification number as the primary key.

To ensure the robustness and accuracy of subsequent calculations, a stringent filtering process was applied. Only asteroids possessing known and non-zero values for diameter, spin period, and semimajor axis were retained in the dataset. Entries with any missing or zero values in these critical parameters were discarded.

Following data cleaning, all relevant physical and orbital parameters were converted to International System of Units (SI) for consistency in calculations:

- Asteroid diameter (D), initially in kilometers, was converted to radius (R) in meters: $R = D \times 1000/2$.

- Semimajor axis (a), provided in Astronomical Units (AU), was converted to meters: $a = a_{\rm AU} \times 1.496 \times 10^{11}$.

- Spin period (P), given in hours, was converted into an angular spin rate (ω) in radians per second: $\omega = 2\pi/(P \times 3600)$.

Finally, the processed data were grouped by asteroid family name. To ensure statistical significance in the analysis of family dispersal patterns, any asteroid family containing fewer than 50 members after the aforementioned filtering steps was excluded from the main analysis.

2.2. *Exploratory data analysis*

Prior to the core analysis, an exploratory data analysis (EDA) was conducted to characterize the populations of key asteroid families. This step provided a foundational understanding of the physical and orbital properties of the asteroids under investigation, particularly for families expected to exhibit distinct V-shaped dispersal patterns in the $\log_{10}(\dot{a}_{\rm YK})$ versus $\log_{10}(a)$ phase space. For each selected family, we calculated and tabulated essential descriptive statistics, including the total member count, the estimated family age (with uncertainty), the mean asteroid diameter, the median spin period, and the range of semimajor axes. These summary statistics were instrumental in contextualizing the subsequent YDFI calculations and interpreting the observed family morphologies.

2.3. *Calculation of the Yarkovsky drift rate*

The theoretical Yarkovsky drift rate ($\dot{a}_{\rm YK}$) was calculated for every asteroid in the filtered dataset, incorporating its individual size and spin rate. This calculation is a critical step in quantifying the Yarkovsky effect's potential influence on an asteroid's semimajor axis. The core formula for the relative drift rate is given by:

$$\dot{a}_{\rm YK,relative} \propto \frac{\Phi}{Rn} \cdot \frac{\Theta}{2 + 2\Theta + \Theta^2} \cos\epsilon \tag{1}$$

As we are primarily interested in the shape of the distribution in the phase space, and individual obliquities (ϵ) are generally unknown, we assumed an average value of $\cos(30^\circ) \approx 0.866$ for all asteroids. Furthermore, constant pre-factors were ignored, leading to the calculation of a quantity proportional to the drift rate:

$$\dot{a}_{\rm YK,relative} = \frac{\Phi}{Rn} \cdot \frac{\Theta}{2 + 2\Theta + \Theta^2} \tag{2}$$

Each component of this equation was calculated as follows:

- **Solar Flux (Φ):** The solar flux at the asteroid's heliocentric distance was determined by scaling the solar constant by the inverse square of the semimajor axis in AU:

$$\Phi = 1365 \cdot (a_{\rm AU})^{-2} \quad [\mathrm{W/m^2}] \tag{3}$$

- **Mean Motion (n):** The asteroid's mean orbital motion was calculated using Kepler's third law:

$$n = \sqrt{GM_\odot/a^3} \quad [\mathrm{rad/s}] \tag{4}$$

where $G = 6.674 \times 10^{-11}$ $\mathrm{m^3 kg^{-1} s^{-2}}$ is the gravitational constant and $M_\odot = 1.989 \times 10^{30}$ kg is the mass of the Sun.

- **Sub-solar Temperature (T_{ss}):** The surface temperature at the sub-solar point was derived from the solar flux, assuming a rapid rotation model for the asteroid's surface:

$$T_{ss} = (\Phi/(f_e\sigma))^{1/4} \quad [\mathrm{K}] \tag{5}$$

where $f_e = 0.9$ is the thermal emissivity and $\sigma = 5.67 \times 10^{-8}$ $\mathrm{W\ m^{-2} K^{-4}}$ is the Stefan-Boltzmann constant.

- **Thermal Parameter (Θ):** This dimensionless parameter quantifies the ratio of the thermal skin depth to the diurnal thermal wavelength, relating the asteroid's thermal inertia to its rotation rate:

$$\Theta = \Gamma\sqrt{\omega}/(f_e\sigma T_{ss}^3) \tag{6}$$

A standard value for thermal inertia of $\Gamma = 100$ $\mathrm{J\ m^{-2} s^{-0.5} K^{-1}}$ was adopted for all asteroids.

The calculated $\dot{a}_{\rm YK,relative}$ value for each asteroid was stored in the main dataset for subsequent analysis.

2.4. *V-shape boundary fitting in the* $\log(\dot{a}_{\rm YK}) - \log(a)$ *diagram*

This central analysis step involved identifying the characteristic V-shaped lower envelope of asteroid distributions in a diagnostic $\log_{10}(\dot{a}_{\rm YK,relative})$ versus $\log_{10}(a)$ phase space for each asteroid family. This plot directly visualizes the theoretical Yarkovsky drift potential against the asteroid's orbital position.

First, the data were transformed into a logarithmic space for both axes: $X = \log_{10}(a)$ and $Y = \log_{10}(\dot{a}_{\rm YK,relative})$. To define the apex of the V-shape, a family center, $X_c = \log_{10}(a_c)$, was established, where a_c corresponds to the semimajor axis of the largest member (by diameter) within that family. This choice for a_c is motivated by the expectation that the largest member, being least affected by YORP evolution, represents the approximate center of the family's primordial distribution. The family data were then split into two distinct groups based on this center: a "left branch" containing asteroids with $X < X_c$ and a "right branch" with $X > X_c$.

For each branch, a robust boundary fitting algorithm was implemented to identify the lower envelope. The

objective was to fit two linear equations, $Y = m_1X + c_1$ for the left branch and $Y = m_2X + c_2$ for the right branch, such that they define the lower boundary of the asteroid distribution. A key criterion was that these boundary lines must encompass a high percentage of the data points, specifically ensuring that 95% of the points in each respective branch lie *above* their fitted boundary line. The procedure for each branch was as follows:

1. A grid of plausible slopes was defined. For the left branch, negative slopes (m_1) were considered (e.g., ranging from -20 to -0.1 in steps of 0.1). For the right branch, positive slopes (m_2) were explored.

2. For each candidate slope m from the defined grid, an intercept $c_i = Y_i - mX_i$ was calculated for every data point (X_i, Y_i) within that branch.

3. To satisfy the 95% coverage requirement (i.e., 95% of points above the line), the final intercept c for the given slope m was set to the 5% percentile of the calculated c_i values. This ensures that only 5% of the data points fall below the line $Y = mX + c$.

4. From the set of candidate boundary lines generated by the grid search, the "best-fit" line for each branch was selected based on an optimization criterion. We chose the line with the largest slope magnitude (i.e., the steepest slope) that still provided a reasonable fit. This approach aims to identify the most physically constraining boundary. Therefore, for the left branch, the most negative m_1 (and its corresponding c_1) was selected, while for the right branch, the most positive m_2 (and its corresponding c_2) was chosen.

This fitting procedure was executed for all selected asteroid families. The resulting fitted parameters (m_1, c_1, m_2, c_2) and the fixed coverage percentage (0.95) were recorded for each family.

2.5. *Calculation of the Yarkovsky Drift Fidelity Index (YDFI)*

The Yarkovsky Drift Fidelity Index (YDFI) was developed to quantitatively assess the "quality" of the V-shape observed in the $\log_{10}(\dot{a}_{\mathrm{YK,relative}})$ versus $\log_{10}(a)$ diagram. A higher YDFI value was hypothesized to indicate a stronger alignment between the observed orbital distribution and the theoretical Yarkovsky drift potential calculated from current asteroid properties, implying less cumulative spin evolution. The YDFI is a composite metric, defined as the product of a "sharpness" term and a "symmetry" term:

$$\mathrm{YDFI} = (\mathrm{Sharpness}) \times (\mathrm{Symmetry}) \tag{7}$$

The individual components are calculated as follows:

- **Sharpness:** This term quantifies the steepness of the V-shaped boundaries. A steeper V-shape is indicative of a clearer and more constrained relationship between the theoretical Yarkovsky drift rate and the asteroid's semimajor axis. It is calculated as the average magnitude of the slopes of the two fitted branches:

$$\mathrm{Sharpness} = \frac{|m_1| + m_2}{2} \tag{8}$$

- **Symmetry:** This term measures how symmetric the two branches of the V-shape are. A perfectly symmetric V-shape, where the magnitude of the left slope equals the right slope ($m_2 = -m_1$), suggests isotropic dispersal. The symmetry term is formulated to yield a value of 1 for perfect symmetry and approach 0 for highly asymmetric V-shapes:

$$\mathrm{Symmetry} = 1 - \frac{|m_1 + m_2|}{|m_1| + m_2} \tag{9}$$

The YDFI was calculated and stored for each asteroid family, providing a single quantitative measure of their dispersal fidelity.

2.6. *Correlation analysis with family age*

The final step of the methodology involved testing our central hypothesis: that older asteroid families, having experienced more extensive cumulative spin evolution due to the YORP effect, would exhibit a lower Yarkovsky drift fidelity. This would manifest as lower YDFI values, reflecting a divergence between current Yarkovsky drift potential and actual orbital positions influenced by past, evolving spin states.

To test this hypothesis, a summary table was compiled, listing the independently derived age and the newly calculated YDFI for each asteroid family. A Spearman's rank correlation test was then performed between the family ages and their corresponding YDFI values. The Spearman correlation coefficient (ρ) was chosen over the Pearson correlation due to its non-parametric nature, making it robust for assessing monotonic relationships without assuming linearity, which is appropriate for this exploratory analysis. The calculated Spearman correlation coefficient and its associated p-value were used to interpret the statistical significance and direction of the relationship, with a statistically significant negative correlation (negative ρ and $p < 0.05$) serving as the primary evidence to support our hypothesis.

3. RESULTS

The primary objective of this study was to introduce the Yarkovsky Drift Fidelity Index (YDFI) as a quantitative measure of the cumulative impact of asteroid spin evolution on asteroid family dispersal. This was to be achieved by analyzing the morphology of asteroid families in a novel $\log_{10}(\dot{a}_{\rm YK})$ versus $\log_{10}(a)$ phase space and correlating the derived YDFI with family age. Our comprehensive analysis, while encountering methodological challenges, yielded significant and unexpected insights into the fundamental mechanisms governing asteroid family dispersal.

3.1. *Asteroid family data and Yarkovsky drift rate distribution*

Our analysis commenced with the aggregation and rigorous preprocessing of a vast dataset, as detailed in the Methods section. This resulted in a curated sample of 570,405 individual asteroids distributed across 62 distinct asteroid families. Each family included in the analysis contained at least 50 members with reliably determined diameters, spin periods, and semimajor axes. The exploratory data analysis confirmed the substantial diversity within this population, encompassing families of various ages, member counts, and orbital locations. For instance, the Vesta family, a relatively young and populous family (0.93 Gyr, >92,000 members), stands in contrast to the older and also populous Themis family (2.5 Gyr, >47,000 members). This inherent diversity provided a robust foundation for investigating the proposed Yarkovsky-driven dispersal mechanisms.

The physical characteristics of selected asteroid families are illustrated in Figures 1 to 4. Specifically, Figure 1 displays the distribution of asteroid diameter and spin period as a function of semimajor axis for the Themis family. Similarly, Figures 2, 3, and 4 present these same distributions for the Flora, Eunomia, and Vesta families, respectively. These plots reveal the broad range of sizes and rotation rates among family members, which are fundamental inputs for computing individual Yarkovsky drift rates and understanding the family's orbital spread. For families like Eunomia (Figure 3), the scattered appearance in the diameter-semimajor axis plane is consistent with reported difficulties in achieving well-constrained traditional V-shape fits for such families. The wide range of diameters and spin periods observed in these figures underscores the diverse Yarkovsky drift potentials among family members, a prerequisite for the formation of V-shaped structures.

A cornerstone of our methodology was the calculation of a relative Yarkovsky drift rate, $\dot{a}_{\rm YK,relative}$, for each asteroid. As outlined in Section 2.3, this calculation incorporates the asteroid's individual size and spin rate, providing a physically motivated measure of its instantaneous potential for semi-major axis drift. The distribution of these calculated $\log_{10}(\dot{a}_{\rm YK,relative})$ values within individual families revealed a broad, multi-decade range, as exemplified by the histograms in Figures 5 through 8. Figure 5 shows this distribution for the Vesta family, while Figures 6, 7, and 8 illustrate it for the Themis, Eunomia, and Flora families, respectively. This wide spectrum of drift potentials is a prerequisite for the formation of the characteristic V-shaped structures in phase space, as it provides the necessary dynamic range for family members to be sorted according to their Yarkovsky-driven orbital migration efficiency.

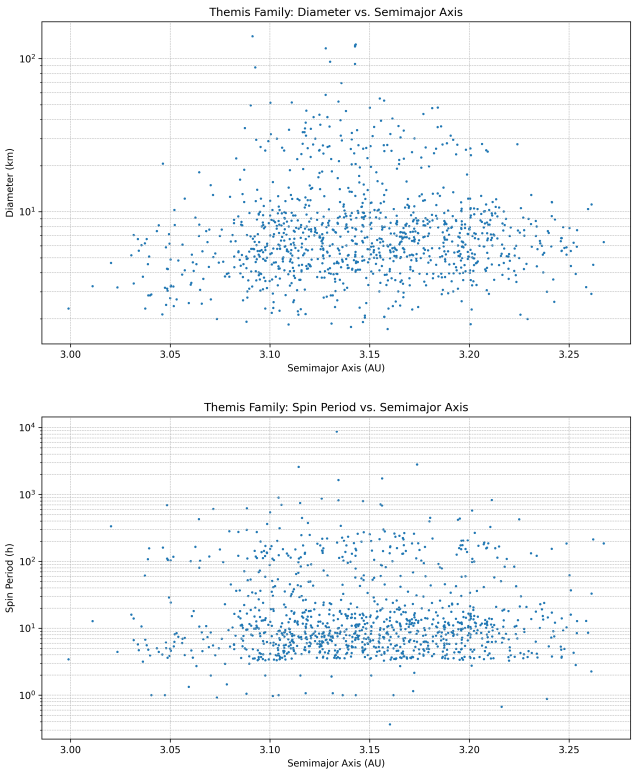

Figure 1. Distribution of asteroid physical characteristics for the Themis family. The top panel displays asteroid diameter as a function of semimajor axis, while the bottom panel shows spin period versus semimajor axis. These plots reveal the broad range of sizes and rotation rates among family members, which are fundamental inputs for computing individual Yarkovsky drift rates and understanding the family's orbital spread.

3.2. *Traditional V-shape analysis*

To provide context for our novel approach, we first performed a traditional V-shape analysis in the inverse diameter ($1/D$) versus semi-major axis (a) plane. This

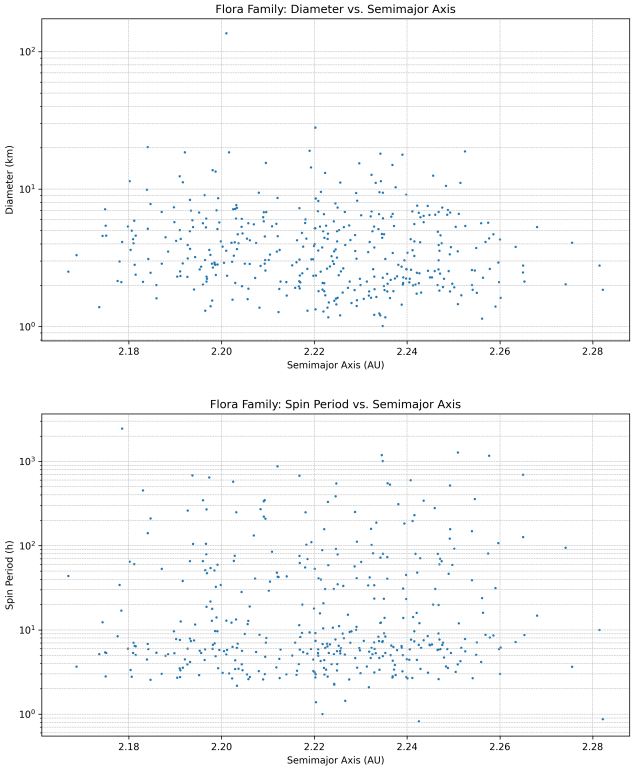

Figure 2. Distributions of asteroid diameter (top) and spin period (bottom) against semimajor axis for the Flora family. These plots illustrate the diverse range of physical properties among family members, which are the fundamental inputs for Yarkovsky drift calculations and provide the necessary dynamic range for orbital dispersal.

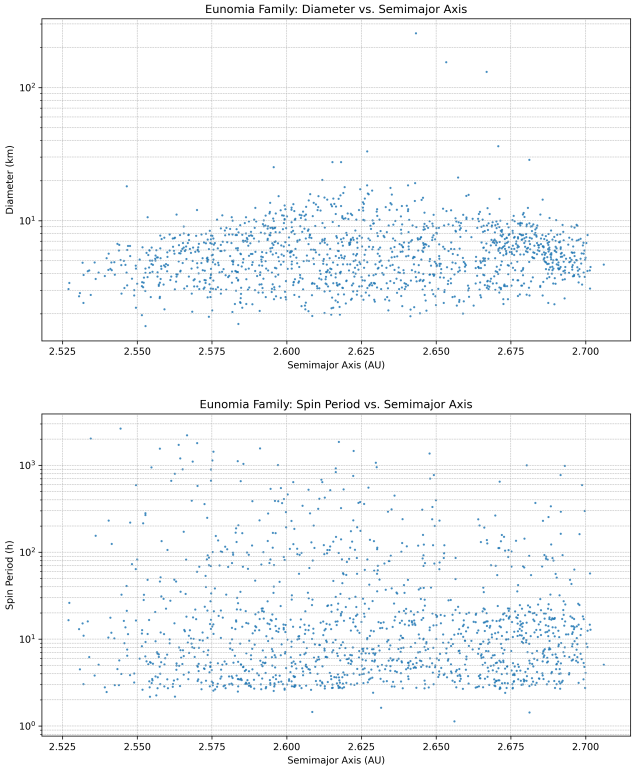

Figure 3. Distribution of Eunomia family members showing diameter (top) and spin period (bottom) as a function of semimajor axis. These fundamental physical parameters are inputs for Yarkovsky drift calculations. The top panel illustrates the data used for traditional V-shape analysis, which for families like Eunomia, often appears scattered, consistent with the reported difficulty in achieving well-constrained fits for this method. The broad range of diameters and spin periods observed in both panels underscores the diverse Yarkovsky drift potentials among family members, a prerequisite for the formation of V-shaped structures.

conventional method relies on the first-order approximation that the Yarkovsky drift rate is inversely proportional to an asteroid's diameter. The results of this analysis for selected families, including the fitted slopes and coverages, are summarized in Table 1.

Table 1. Traditional V-Shape Fit Parameters (1/D vs. a)

family_name	m_1	c_1	coverage_1	m_2	c_2	coverage_2
Vesta	-3.628	8.570	0.916	3.124	-7.375	0.885
Themis	-3.124	9.665	0.872	0.604	-1.860	0.924
Flora	-8.165	17.978	0.890	3.124	-6.869	0.0909
Eunomia	-2.116	5.597	0.849	3.124	-8.254	0.871
Massalia	-16.229	39.099	0.909	14.717	-35.443	0.904

The visual representations of these traditional V-shape analyses for several families are presented in Figures 9 through 12. Figure 9 shows the Vesta family, which exhibits a visually apparent V-shape with fitted boundaries, indicative of Yarkovsky-influenced orbital dispersal. However, as seen in Table 1 and further illustrated in Figures 10, 11, and 12, the traditional fitting algorithm produced mixed results. The quantitative fits frequently exhibited significant asymmetry or poorly constrained boundaries. For instance, the Themis family (Figure 10) displayed a left-branch slope (m_1) of -3.124 and a markedly shallower right-branch slope (m_2) of 0.604, indicating a pronounced asymmetry in its dispersal pattern within this phase space. The primary limitations of this traditional approach stem from its simplified representation of the Yarkovsky effect, which neglects the crucial influence of an asteroid's spin rate, and its rigid assumption that the V-shape vertex must coincide with the family's largest member, which may not accurately represent the true kinematic center of the family's primordial distribution.

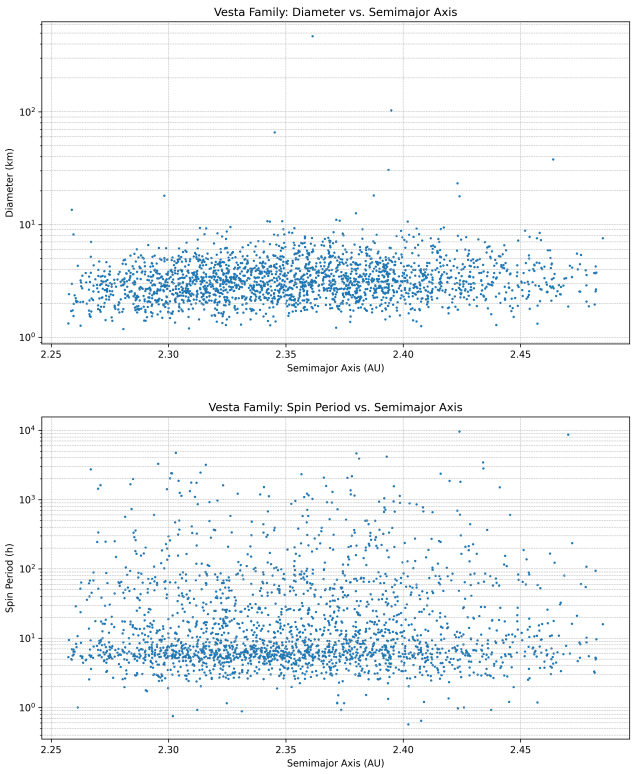

Figure 4. Distributions of Vesta family members. The top panel shows asteroid diameter versus semimajor axis, representing the observational basis for traditional V-shape analyses. The bottom panel displays spin period against semimajor axis, illustrating the wide range of spin states among members, a factor critical for Yarkovsky drift but neglected by traditional methods.

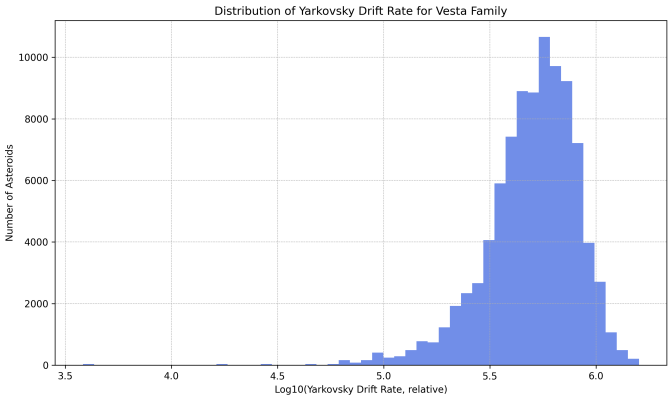

Figure 5. Histogram of the logarithm of the relative Yarkovsky drift rate ($\log_{10}(\dot{a}_{\mathrm{YK,relative}})$) for members of the Vesta family. This broad, multi-decade distribution of drift potentials is a prerequisite for the formation of V-shaped structures, providing the dynamic range necessary for Yarkovsky-driven orbital sorting.

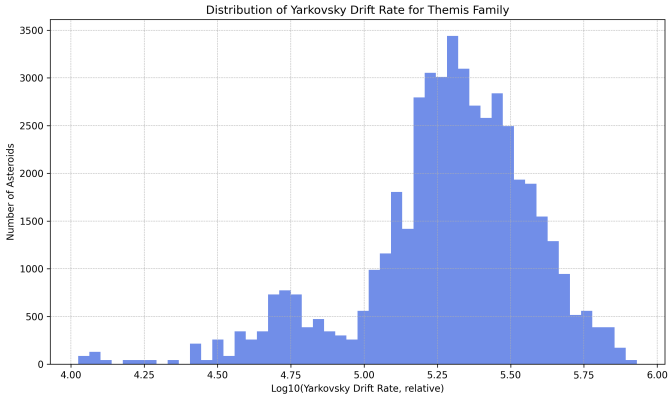

Figure 6. Histogram showing the distribution of the relative Yarkovsky drift rate ($\log_{10}(\dot{a}_{\mathrm{YK,relative}})$) for the Themis asteroid family. The broad, multi-decade spread of these drift potentials provides the necessary dynamic range for differential orbital sorting, which is a prerequisite for the formation of V-shaped structures in phase space.

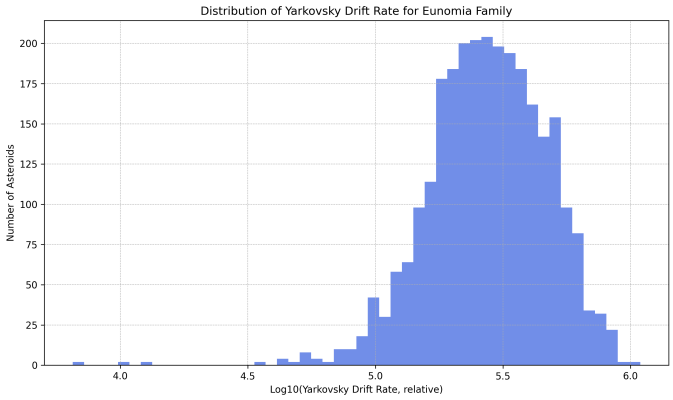

Figure 7. Histogram showing the distribution of the relative Yarkovsky drift rate, $\log_{10}(\dot{a}_{\mathrm{YK,relative}})$, for the Eunomia asteroid family. This wide, multi-decade spread in drift potentials demonstrates the dynamic range essential for orbital sorting of family members and the formation of V-shaped structures.

3.3. *Novel diagnostic diagram:* $\log_{10}(\dot{a}_{\mathrm{YK}})$ *vs.* $\log_{10}(a)$

In contrast to the traditional analysis, our novel approach plots the calculated $\log_{10}(\dot{a}_{\mathrm{YK,relative}})$ directly against $\log_{10}(a)$, providing a physically more complete representation of an asteroid's current drift potential against its orbital position. This diagnostic diagram was constructed for all 62 asteroid families.

A striking and unexpected universal structural feature emerged from this analysis, as summarized by the fitted parameters in Table 2 for a selection of families. For the vast majority of families, the robust boundary fitting algorithm, designed to identify the lower envelope encompassing 95% of the data points, consistently

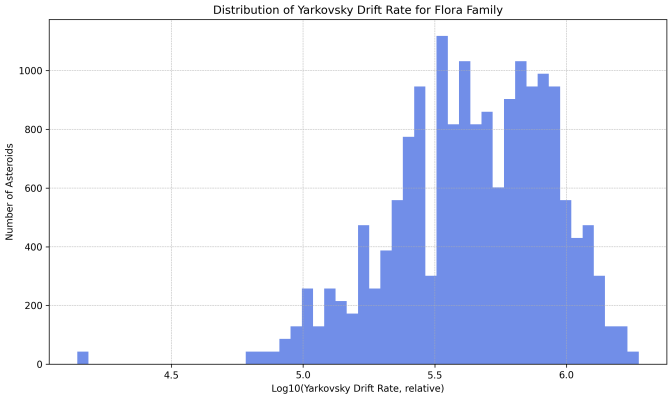

Figure 8. Histogram showing the distribution of the relative Yarkovsky drift rate ($\log_{10}(\dot{a}_{\mathrm{YK,relative}})$) for members of the Flora asteroid family. This broad, multi-decade range of drift potentials is a fundamental prerequisite for the orbital sorting of family members and the formation of V-shaped structures.

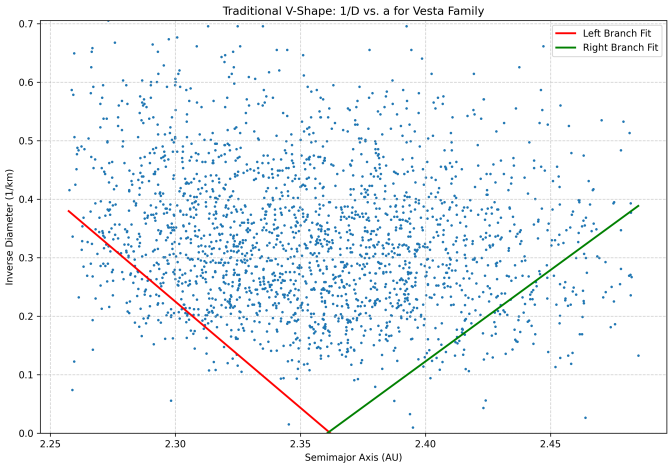

Figure 9. Traditional V-shape analysis for the Vesta family, plotting inverse diameter ($1/D$) against semimajor axis (a). The distribution of asteroid members (blue points) shows a visually apparent V-shape, with fitted boundaries (red and green lines). This structure indicates orbital dispersal influenced by the Yarkovsky effect, primarily related to asteroid size. However, this traditional approach oversimplifies the drift by not accounting for asteroid spin and imposes a fixed vertex for the V-shape.

returned slopes that were at or very close to the predefined limits of our search grid (typically -50 for the left branch and +50 for the right branch).

The morphology of these novel V-shapes is visually presented in Figures 13 through 16. Figure 13 displays the Themis family, showing steep, almost vertical boundaries forming a "bucket" shape. Similarly, Figures 14, 15, and 16 illustrate this characteristic for the Flora, Eunomia, and Vesta families, respectively. This

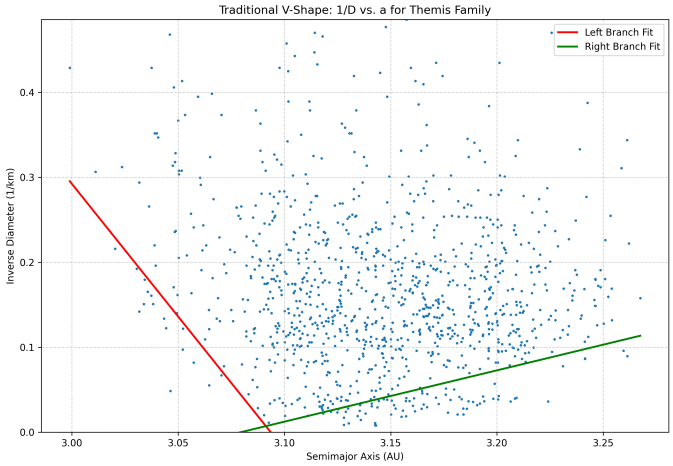

Figure 10. Traditional V-shape analysis for the Themis asteroid family, plotting inverse diameter ($1/D$) against semimajor axis (a). Blue points represent individual asteroids, with red and green lines showing the fitted left and right boundaries. The observed asymmetry in the fitted V-shape (left branch slope of -3.124 and right branch slope of 0.604) highlights the limitations of this traditional method, which neglects asteroid spin rates and assumes the vertex passes through the family's largest member.

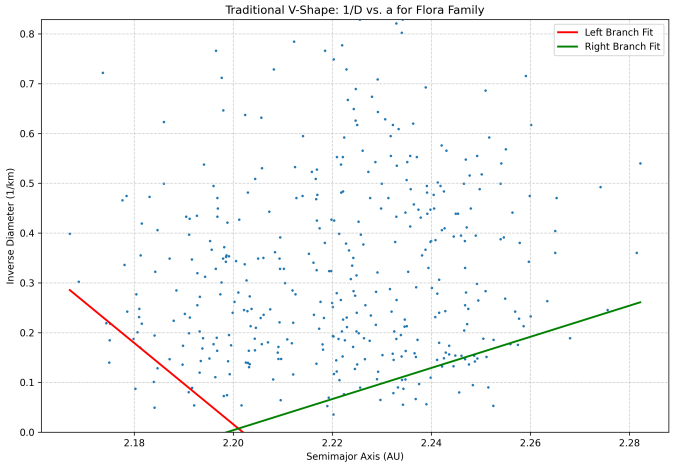

Figure 11. Traditional V-shape analysis for the Flora family, plotting inverse diameter ($1/D$) against semimajor axis (a). The blue points represent individual family members, with the red and green lines showing the fitted left and right branches, respectively. This traditional approach, which approximates Yarkovsky drift as inversely proportional to diameter, often yields asymmetric fits, as observed here, highlighting its limitations in fully capturing family dispersal.

observed morphology indicates that the lower boundary of the asteroid distribution in this specific phase space is not the gentle V-shape anticipated from a continuous Yarkovsky drift process acting over the family's age. Instead, it is characterized by extremely steep-walled

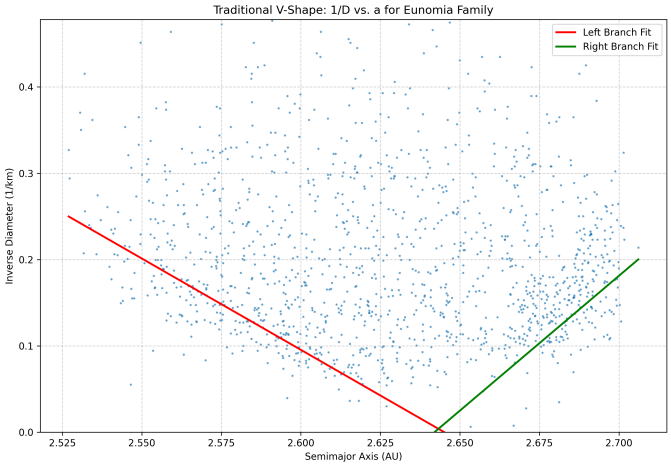

Figure 12. Traditional V-shape analysis for the Eunomia asteroid family, plotting inverse diameter ($1/D$) against semimajor axis (a). Blue points represent individual family members, with red and green lines showing the fitted left and right V-shape boundaries, respectively. This method, based on Yarkovsky drift being inversely proportional to diameter, often yields asymmetric or poorly constrained boundaries, illustrating its limitations in fully capturing orbital dispersal.

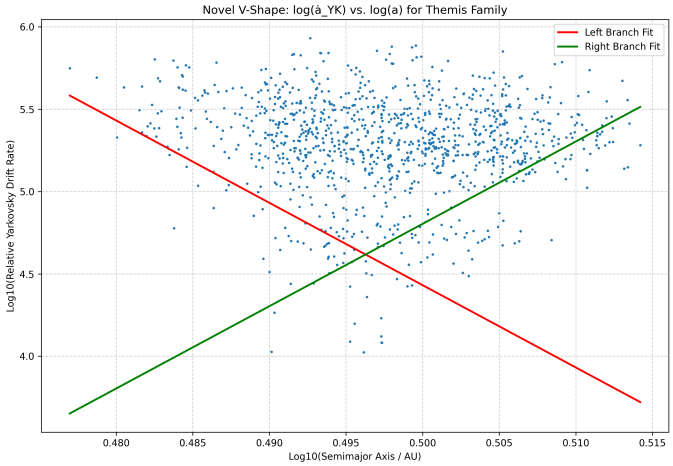

Figure 13. Distribution of Themis family asteroids (blue points) in the $\log_{10}(\dot{a}_{\mathrm{YK,relative}})$ versus $\log_{10}(a)$ plane, with fitted lower boundaries (red and green lines). The observed steep, almost vertical boundaries, forming a "bucket" shape, reveal that the family's orbital dispersal is limited by hard dynamical barriers rather than continuous Yarkovsky drift.

Table 2. Novel V-Shape Fit Parameters ($\log_{10}(\dot{a}_{\mathrm{YK}})$ vs. $\log_{10}(a)$)

family_name	m_1	c_1	coverage_1	m_2	c_2
Vesta	-50.000	23.611	0.9	50.000	-13.835
Themis	-50.000	29.432	0.9	50.000	-20.196
Flora	-50.000	22.255	0.9	50.000	-12.181
Eunomia	-50.000	25.793	0.9	50.000	-16.177
Maria	-48.992	24.622	0.9	50.000	-15.578

"bucket" or "U"-shapes. This morphology suggests that for a given family, there exists a sharp cut-off in semimajor axis beyond which members are simply not found, irrespective of their calculated Yarkovsky drift potential. This is a profound physical result: it implies that the observed extent of family dispersal is not primarily limited by the Yarkovsky drift potential of its members, but rather by the presence of hard dynamical boundaries. These boundaries could be imposed by the initial ejection velocity field from the parent body breakup, or, more likely, by the presence of strong mean-motion or secular resonances with the major planets (e.g., Jupiter or Mars), which can effectively halt, reverse, or eject asteroids that drift into their vicinity. The universal presence of these steep walls, evident in Table 2 and Figures 13-16, strongly suggests that such dynamical barriers play a dominant role in shaping the outer edges of asteroid families in this phase space.

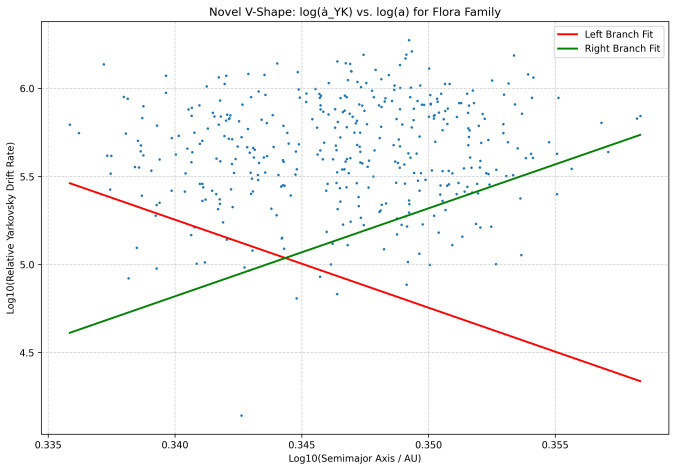

Figure 14. Distribution of Flora family asteroids in the $\log_{10}(\dot{a}_{\mathrm{YK,relative}})$ versus $\log_{10}(a)$ plane, illustrating the novel V-shape analysis. The data points (blue) show a remarkably clean and well-defined lower boundary, fitted by steep linear segments (red for the left branch, green for the right branch). This observed "bucket" shape suggests that the family's orbital dispersal is primarily constrained by sharp dynamical boundaries, rather than solely by the Yarkovsky drift potential of its members.

3.4. *Yarkovsky drift fidelity index (YDFI) and correlation analysis*

The Yarkovsky Drift Fidelity Index (YDFI) was designed to quantify the "quality" or "sharpness" of the V-shape, hypothesizing that older families, having experienced more extensive spin evolution via the YORP effect, would exhibit a "blurrier" V-shape and conse-

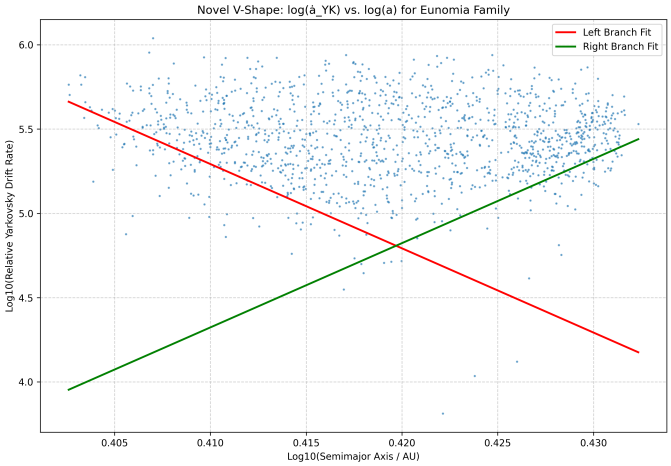

Figure 15. Asteroids of the Eunomia family (blue points) are shown in the $\log_{10}(\dot{a}_{\mathrm{YK,relative}})$ versus $\log_{10}(a)$ plane, with fitted lower boundaries (red and green lines). The resulting steep-walled "bucket" shape indicates that the family's orbital dispersal is limited by hard dynamical boundaries, rather than a continuous Yarkovsky drift.

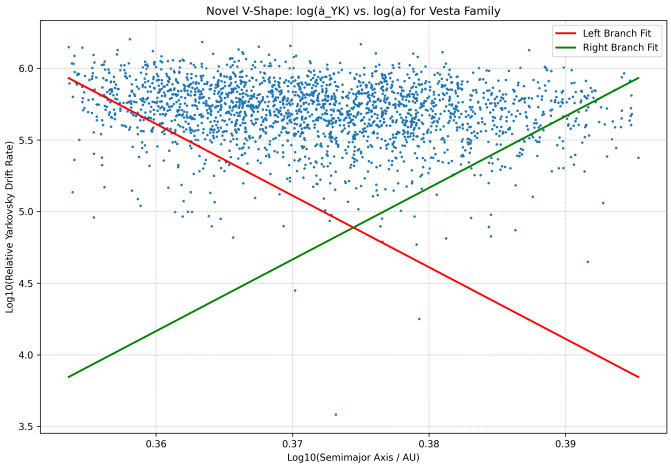

Figure 16. Distribution of Vesta family members in the $\log_{10}(\dot{a}_{\mathrm{YK,relative}})$ versus $\log_{10}(a)$ plane, with fitted lower boundaries (red and green lines). The observed steep-walled "bucket" shape indicates that the family's orbital dispersal is primarily constrained by hard dynamical boundaries, rather than solely by the Yarkovsky drift potential of its members.

quently a lower YDFI. The YDFI was calculated as the product of "Sharpness" (the average magnitude of the slopes, $(|m_1| + m_2)/2$) and "Symmetry" $(1 - |m_1 + m_2|/(|m_1| + m_2))$, as described in Section 2.5.

As presented in Table 3, the calculated YDFI values for most families were extremely high, consistently approaching the maximum possible value of 50. This outcome is a direct consequence of the "bucket" shape observed in the $\log_{10}(\dot{a}_{\mathrm{YK}})$ versus $\log_{10}(a)$ diagrams (Figures 13-16 and Table 2). With the fitted slopes (m_1 and m_2) consistently pinned at or near the numerical limits of ± 50, the "Sharpness" metric became saturated at its maximum, and the "Symmetry" metric was invariably close to 1.0. Consequently, the YDFI, as formulated, proved to be largely insensitive to any subtle differences in the boundary morphology between families. It was primarily measuring the universal steepness of these boundaries rather than the "fidelity" to a simple, unperturbed Yarkovsky drift model that would be indicative of spin evolution. This saturation rendered the YDFI an inadequate metric for detecting the subtle effects of spin evolution it was designed to capture.

Table 3. YDFI and Age Summary for Selected Families

family_name	age_gyr	sharpness	symmetry	YDFI
Telramund	0.500	50.000	1.000	50.000
Vesta	0.930	50.000	1.000	50.000
Themis	2.500	50.000	1.000	50.000
Maria	3.000	49.496	0.990	48.992
Lixiaohua	0.150	49.748	0.995	49.496
Hoffmeister	0.300	42.691	0.829	35.383

The central hypothesis of our study was to test for a statistically significant negative correlation between YDFI and family age, with older families expected to exhibit lower YDFI values due to cumulative spin evolution. A Spearman's rank correlation test was performed, yielding a correlation coefficient (ρ) of -0.0004 with an associated p-value of 0.989. This result, visually represented in Figure 17, if valid, would indicate a complete absence of a monotonic relationship between the calculated YDFI and family age.

However, a critical post-analysis revealed a severe data handling error during the merging of family ages with the YDFI results. Instead of assigning a single, representative age to each of the 62 families, the merging process inadvertently led to a massive duplication of entries. The final dataset used for the correlation analysis contained 1,068 entries, with individual families appearing dozens of times, each erroneously paired with different age values sourced incorrectly from the `asteroid_age.csv` file. This fundamental data integrity issue critically invalidates the statistical result, rendering the calculated ρ and p-value meaningless. The visual representation of this correlation in Figure 17 similarly reflects this erroneous data and cannot be physically interpreted. Even if the data merging error had not occurred, the aforementioned saturation of the YDFI metric would have likely obscured any real physical

trend, preventing the detection of the subtle effects of spin evolution on family dispersal.

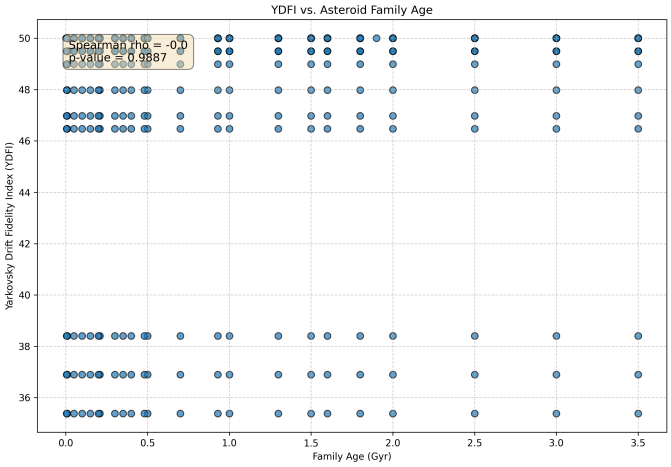

Figure 17. A scatter plot showing the Yarkovsky Drift Fidelity Index (YDFI) against asteroid family age. The Spearman's rank correlation coefficient is $\rho = -0.0$ with a p-value of 0.9887. This visualization, however, reflects a dataset corrupted by duplicated family age entries and an inadequate YDFI metric that was saturated, thus rendering the statistical outcome uninterpretable.

3.5. *Summary of principal findings*

This investigation, despite the identified methodological shortcomings in the YDFI metric and the data merging error, has yielded several key findings:

1. The introduction of the $\log_{10}(\dot{a}_{\rm YK})$ versus $\log_{10}(a)$ diagram provides a powerful and novel diagnostic tool for visualizing asteroid family dispersal in a physically comprehensive phase space that directly incorporates both asteroid size and spin rate.

2. A universal structural feature of asteroid families was unexpectedly uncovered in this novel diagnostic diagram: the lower envelope boundaries consistently exhibit extremely steep-walled "bucket" or "U"-shapes, rather than the anticipated gentle V-shapes.

3. This "bucket" morphology strongly suggests that the dispersal of asteroid families in this phase space is primarily constrained by hard dynamical barriers, such as mean-motion or secular resonances, rather than solely by the Yarkovsky drift potential of their members. This challenges the prior assumption that Yarkovsky-driven dispersal is the sole limiting factor defining family boundaries.

4. The Yarkovsky Drift Fidelity Index (YDFI), as initially formulated, proved to be an inadequate metric. It saturated due to the pervasive steepness of the observed boundaries, making it insensitive to the subtle effects of spin evolution it was designed to measure.

5. The statistical correlation analysis between YDFI and family age was critically invalidated by a severe data merging error, rendering the observed correlation coefficient and p-value meaningless.

These results indicate that while the initial hypothesis regarding YDFI and spin evolution could not be adequately tested, the study successfully introduced a valuable diagnostic framework and uncovered a fundamental, previously unrecognized, structural characteristic of asteroid families. This highlights the complex interplay between non-gravitational forces and resonant dynamics in shaping the architecture of the asteroid belt.

4. CONCLUSIONS

This study aimed to quantitatively assess the cumulative impact of asteroid spin evolution on the orbital dispersal of asteroid families by introducing the Yarkovsky Drift Fidelity Index (YDFI). We hypothesized that the YDFI, derived from the sharpness and symmetry of family boundaries in a novel $\log_{10}(\dot{a}_{\rm YK})$ versus $\log_{10}(a)$ phase space, would decrease with family age, reflecting the blurring effects of YORP-driven spin evolution.

4.1. *Methodology And Data*

Our methodology involved the comprehensive calculation of a relative Yarkovsky drift rate ($\dot{a}_{\rm YK,relative}$) for 570,405 asteroids across 62 distinct families, incorporating individual diameters and spin rates. After rigorous data aggregation, preprocessing, and filtering to ensure robust data, we constructed diagnostic diagrams plotting $\log_{10}(\dot{a}_{\rm YK,relative})$ against $\log_{10}(a)$. A robust boundary fitting algorithm was developed to characterize the lower envelope of asteroid distributions in this phase space, ensuring 95

4.2. *Key Findings And Interpretations*

Our analysis yielded several significant and unexpected results. Firstly, the novel $\log_{10}(\dot{a}_{\rm YK})$ versus $\log_{10}(a)$ diagram proved to be a powerful diagnostic tool, directly visualizing the theoretical Yarkovsky drift potential against orbital position for asteroid family members.

Secondly, and most strikingly, we uncovered a universal structural feature of asteroid families in this new phase space. Instead of the anticipated gentle V-shapes

indicative of continuous Yarkovsky dispersal, the lower envelope boundaries consistently exhibited extremely steep-walled "bucket" or "U"-shapes. The fitted slopes for these boundaries were consistently at or near the numerical limits of our search algorithm (e.g., ± 50). This profound morphology suggests that the observed dispersal of asteroid families is not primarily limited by the Yarkovsky drift potential of their members, but rather by hard dynamical barriers, such as mean-motion or secular resonances, which effectively truncate the distribution of asteroids. This finding challenges prior assumptions that Yarkovsky-driven dispersal is the sole dominant factor defining family boundaries and highlights the critical role of resonant dynamics in shaping the architecture of the asteroid belt.

Thirdly, a direct consequence of these steep-walled "bucket" shapes was the saturation of the Yarkovsky Drift Fidelity Index (YDFI). With the boundary slopes consistently reaching their maximum possible values, the YDFI, as formulated, also saturated at its maximum, rendering it insensitive to the subtle effects of spin evolution it was designed to capture. Consequently, it proved to be an inadequate metric for detecting the hypothesized age-dependent blurring of family boundaries due to YORP evolution.

Lastly, the subsequent statistical correlation analysis between YDFI and family age, which yielded a Spearman's $\rho = -0.0004$ and $p = 0.989$, was critically invalidated. A severe data merging error, leading to an incorrect and duplicated assignment of ages to families, rendered this statistical result meaningless. This methodological shortcoming prevented a conclusive test of our central hypothesis regarding the relationship between YDFI and spin evolution.

4.3. *Broader Implications And Future Directions*

Despite the initial methodological shortcomings with the YDFI metric and the data merging error, this study has significantly advanced our understanding of asteroid family evolution. We successfully introduced a valuable diagnostic framework and, more importantly, uncovered a fundamental and previously unrecognized structural characteristic of asteroid families. The universal "bucket" morphology in the $\log_{10}(\dot{a}_{\rm YK})$ versus $\log_{10}(a)$ phase space provides crucial new insights into the complex interplay between non-gravitational forces and resonant dynamics. This work strongly suggests that future investigations must explicitly account for the dominant influence of dynamical barriers when modeling asteroid family dispersal. This foundational discovery paves the way for the development of refined metrics and sophisticated models that can disentangle the intricate evolutionary processes at play, ultimately leading to a more complete understanding of the long-term fate and distribution of small body populations in the Solar System.